

Correction to “Localized gravity/topography admittance and correlation spectra on Mars: Implications for regional and global evolution”

Patrick J. McGovern, Sean C. Solomon, David E. Smith, Maria T. Zuber, Mark Simons, Mark A. Wieczorek, Roger J. Phillips, Gregory A. Neumann, Oded Aharonson, and James W. Head

Received 27 April 2004; published 20 July 2004.

INDEX TERMS: 6225 Planetology: Solar System Objects: Mars; 5417 Planetology: Solid Surface Planets: Gravitational fields (1227); 5430 Planetology: Solid Surface Planets: Interiors (8147); 5418 Planetology: Solid Surface Planets: Heat flow; 8120 Tectonophysics: Dynamics of lithosphere and mantle—general; **KEYWORDS:** gravity, Mars, thermal evolution

Citation: McGovern, P. J., S. C. Solomon, D. E. Smith, M. T. Zuber, M. Simons, M. A. Wieczorek, R. J. Phillips, G. A. Neumann, O. Aharonson, and J. W. Head (2004), Correction to “Localized gravity/topography admittance and correlation spectra on Mars: Implications for regional and global evolution,” *J. Geophys. Res.*, 109, E07007, doi:10.1029/2004JE002286.

1. Introduction

[1] In the paper “Localized gravity/topography admittance and correlation spectra on Mars: Implications for regional and global evolution” by Patrick J. McGovern, Sean C. Solomon, David E. Smith, Maria T. Zuber, Mark Simons, Mark A. Wieczorek, Roger J. Phillips, Gregory A. Neumann, Oded Aharonson, and James W. Head (*Journal of Geophysical Research*, 107(E12), 5136, doi:10.1029/2002JE001854, 2002), the thickness of the lithosphere and lithospheric heat flow for a number of regions of Mars and as functions of time were inferred on the basis of gravity/topography admittance spectra. Observed admittances, derived from spherical harmonic expansions localized with the scheme of *Simons et al.* [1997], were compared with those predicted from models for the flexural response to lithospheric loading [e.g., *Turcotte et al.*, 1981]. Gravity was calculated according to the finite-amplitude scheme of *Wieczorek and Phillips* [1998]. Estimates for the thickness of the elastic lithosphere T_e at the time of loading for each region were converted to equivalent thermal gradient dT/dz and heat flux q by means of an elastic-plastic stress-envelope formalism [*McNutt*, 1984]. Here we describe a correction required in the calculation of the modeled gravity anomalies; we report new estimates of T_e , load density ρ_l , dT/dz , and q from corrected model admittances; and we discuss the implications of the new results.

[2] The source of the required correction is a difference in reference radius values. As defined by *McGovern et al.* [2002], the planetary shape was taken to equal the radius from the center of mass of Mars to the Martian surface expressed as a spherical harmonic expansion and referenced to the mean equatorial radius $R_{eq} = 3396$ km:

$$S(\theta, \phi) = \sum_{ilm} S_{ilm} Y_{ilm}(\theta, \phi), \quad (1)$$

where $Y_{ilm}(\theta, \phi)$ is the fully normalized spherical harmonic of degree l and order m , i takes the value 1 or 2 for the $\cos(m\phi)$ and $\sin(m\phi)$ terms, respectively, θ is colatitude, and ϕ is longitude. The natural reference for the harmonic expansion of the radius, however, is the mean planetary radius R_p . The sole term accounting for the difference between R_{eq} and R_p is the degree-zero coefficient S_{100} of the radius field (magnitude -6.5 km). This point is important because R_{eq} was chosen as the observation radius r_{obs} in the finite-amplitude gravity calculation, after *Wieczorek and Phillips* [1998]. (The gravity field used in the original paper, mgm1025, from *Lemoine et al.* [2001], was originally referenced to a radius of 3397 km, but the field was downward continued to R_{eq} in the calculations of *McGovern et al.* [2002].) Degree-zero coefficients were not used in the flexure calculations or the finite-amplitude gravity calculations of *McGovern et al.* [2002]. Thus the theoretical gravity calculated from the expansion of S did not properly account for the difference between R_p and R_{eq} . In effect, the gravity signal was not upward continued correctly from R_p to R_{eq} , and therefore the modeled gravity signals and admittances calculated by *McGovern et al.* [2002] were overestimates. Fortunately, the gravity calculated from subsurface density interfaces was properly upward continued to R_{eq} , so the introduced error tends to decrease with increasing contribution of subsurface density interfaces (i.e., with decreasing T_e).

[3] We have recalculated the model admittances for all regions treated by *McGovern et al.* [2002] with the corrected upward continuation procedure but with all other aspects of the methodology unchanged. The observed, original model, and recalculated model admittances for three illustrative regions of Mars are shown in Figure 1. The effect of including the omitted upward continuation is seen to be a reduction in the magnitudes of the modeled gravity and admittance; this reduction increases with increasing spherical harmonic degree l and tends to introduce a falloff in model admittance with increasing l (Figure 1). A summary of the revised best fitting

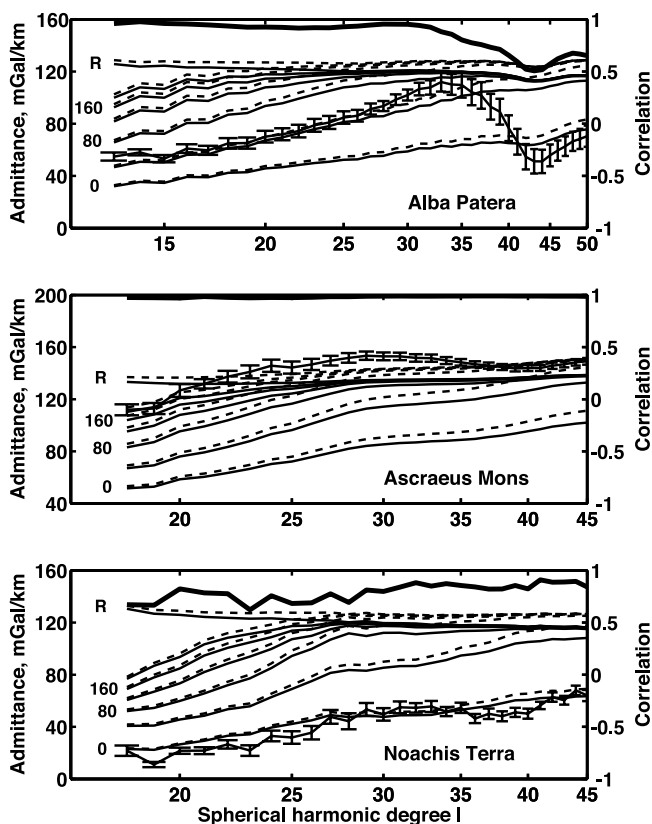


Figure 1. Gravity/shape admittance and correlation spectra versus spherical harmonic degree l for (from top to bottom) Alba Patera (window center at 42°N , 249°E), for harmonic window width $L_{win} = 10$, and Ascraeus Mons (11.5°N , 256°E) and Noachis Terra (35°S , 26°E), for $L_{win} = 15$. Left vertical axis: Curves with errors bars display admittances from observed gravity and shape fields, together with formal errors. Admittances from observed shape and gravity determined from models of thin-spherical-shell flexure are shown as dashed curves for the original calculations and solid curves for the corrected admittances. Following the practice of *McGovern et al.* [2002], nominal model values (given in Table 1 of that paper) are used in all cases, including density $\rho_1 = 2900 \text{ kg/m}^3$, which differs from the best fit densities (Table 1) determined here for the features shown. Calculated admittance curves are for an elastic lithosphere thickness T_e varying from 0 to 200 km (bottom to top) in 40-km increments as well as for a completely uncompensated model (i.e., infinitely rigid lithosphere, labeled “R”). Right vertical axis: Thick solid curves depict the correlation between the observed gravity and shape fields. See color version of this figure in the HTML.

parameter values (T_e , dT/dz , q , and ρ_1) for all regions is given in Table 1.

2. Corrected Results

2.1. Volcanoes and Volcanic Rises

[4] Recalculation of gravity/topography admittances significantly increases the best fit densities of the mate-

rial loading the lithosphere at large Martian volcanoes and volcanic provinces [*Belleguic et al.*, 2004]. As was found earlier [*McGovern et al.*, 2002], the Tharsis Montes have higher best fit densities than Olympus Mons, with Arsia Mons having the highest. However, the corrected best fit densities for all these edifices are greater by several hundred kg/m^3 (Table 1) than the results of *McGovern et al.* [2002]. The new density estimates more closely match the densities of Martian basaltic meteorites [e.g., *Neumann et al.*, 2004] and agree with other recent estimates of densities for Martian volcanoes [*Belleguic et al.*, 2004; *Neumann et al.*, 2004].

[5] On the basis of the revised calculations, the ranges of allowable values for the thickness of the elastic lithosphere T_e beneath the large volcanoes (calculated with the best fit densities) have tended to expand, particularly the lower limits [*Belleguic et al.*, 2004]. For example, the lower bound on T_e at Olympus Mons is 70 km instead of 140 km (Table 1), although there is independent evidence from the absence of circumferential extensional faulting that the latter figure is a more reasonable lower bound [*Thurber and Toksöz*, 1978]. Estimates for the thickness of the elastic lithosphere beneath Ascraeus and Pavonis Montes are substantially lower, such that near-isostatic values are allowed (Table 1). Nonetheless, the best fit models have finite elastic thicknesses. In particular, the best fit model for Ascraeus Mons has a root mean square misfit of 1.5 mGal/km (at $T_e = 40$ km), well below the very conservative 5 mGal/km acceptance criterion adopted by *McGovern et al.* [2002], a figure that allowed for an essentially Airy model near the limiting value. If we instead adopt the criterion of *Nimmo* [2002], that models be rejected if the misfit is greater than a factor of 1.5 times the best fit value, we obtain bounds of $T_e = 32\text{--}46$ km at Ascraeus Mons and $12\text{--}78$ km at Pavonis Mons. Our revised estimates of T_e for the Elysium Rise now bracket the value (29 km, no uncertainty quoted) found by *McKenzie et al.* [2002].

2.2. Valles Marineris

[6] For the three sites in Valles Marineris, our best fit densities are slightly higher, and the ratio f of subsurface to surface loading is slightly lower (Table 1), than those of *McGovern et al.* [2002]. The lower bounds on elastic thickness are significantly less at Candor Chasma but only slightly less at Hebes and Capri Chasmata. The trend of increasing subsurface loading with increasing proximity to Tharsis found by *McGovern et al.* [2002] still holds, supporting the proposed scenario for the association of Valles Marineris formation with intrusive activity.

2.3. Southern Highlands

[7] As found by *McGovern et al.* [2002], admittances in the southern highlands of Mars are best fit by models exhibiting Airy isostasy ($T_e = 0$). Because such models require substantial compensation at the crust-mantle boundary, the error in calculating the gravity due to surface relief affected these results the least. Upper limits on elastic thickness for Noachian-aged

Table 1. Summary of Thermal Gradient and Heat Flux Estimates

| Feature | Surface Age ^a | T_e , km | Thermal Gradient, K/km | Heat Flux, mW/m ² | L_{win} | l Range for Fit | Load Density ^b ρ_l , kg/m ³ | Bottom Loading, f |
|--|--------------------------|------------|------------------------|------------------------------|-----------|-------------------|---|---------------------|
| Olympus Mons ^c | A | >70 | <8 | <24 | 10 | 16–50 | 3150 ^d | 0 |
| Ascraeus Mons ^{c,e} | A | 2–80 | 5–55 | 13–140 | 15 | 18–45 | 3250 ^d | 0 |
| Pavonis Mons ^{c,e} | A | <100 | >5 | >13 | 15 | 18–35 | 3250 ^d | 0 |
| Arsia Mons ^{c,e} | A | >20 | <10 | <28 | 15 | 28–45 | 3300 ^d | 0 |
| Alba Patera ^{c,e} | A-H | 38–65 | 5.5–16 | 16–40 | 10 | 13–35 | 2950 ^d | 0–0.1 |
| Elysium Rise ^c | A-H | 15–45 | 6–13 | 15–33 | 10 | 22–50 | 3250 ^d | 0 |
| Hebes Chasma ^f | A-H | >60 | <10 | <28 | 15 | 18–45 | 2900 | 0.4–0.7 |
| Hebes Chasma ^{f,g,h} | A-H | 60–120 | 5–9 | 17–25 | 15 | 18–45 | 2100–2300 ^d | 0 |
| Candor Chasma ^f | A-H | >120 | <6 | <20 | 15 | 18–45 | 2900 | 0.5 |
| Candor Chasma ^{f,g,h} | A-H | 80–200 | 3–7.5 | 11–23 | 15 | 18–45 | 2200 ^d | 0 |
| Capri Chasma ^f | A-H | >110 | <6 | <20 | 15 | 18–45 | 2900 | 0.2–0.3 |
| Capri Chasma ^{f,g,h} | A-H | >100 | <7 | <23 | 15 | 18–45 | 2500 ^d | 0 |
| Solis Planum ^{f,i} | H | 24–37 | 8–14 | 20–35 | 10 | 13–30 | 2900 | 0 |
| Hellas south rim ^{f,i} | H-N | 20–31 | 10–16 | 25–40 | 15 | 18–45 | 2900 | 0 |
| Hellas south rim ^{e,f,j} | H-N | 40–120 | 6–11 | 20–28 | 15 | 18–45 | 2900 | 0–0.4 |
| Hellas west rim ^{f,i} | H-N | <20 | >12 | >30 | 15 | 18–40 | 2650 ^d | 0 |
| Hellas basin ^{f,i} | N | <13 | >14 | >35 | 5 | 8–55 | 2750 ^d | 0 |
| Noachis Terra ^{f,i} | N | <12 | >20 | >50 | 15 | 18–45 | 2800 ^d | 0 |
| Northeastern Terra Cimmeria ^{f,i} | N | <12 | >19 | >48 | 15 | 18–40 | 2950–3000 ^d | 0 |
| Northeastern Arabia Terra ^{f,i} | N | <16 | >17 | >43 | 15 | 18–40 | 2500 ^d | 0 |

^aThe letters A, H, and N refer to Amazonian, Hesperian, and Noachian epochs, respectively.

^bLoad density varied in increments of 50 kg/m³ unless otherwise noted.

^cCrustal density ρ_c taken to be equal to nominal value (2900 kg/m³, Table 1).

^dBest fit density.

^eParameter ranges reflect the possibility that lithospheric ductile strength may be limited by that of either diabase or olivine.

^fCrustal density ρ_c taken to be equal to load density ρ_l .

^gLoad density varied in increments of 100 kg/m³.

^hAlternate solution with low surface density, $f = 0$.

ⁱDuctile strength taken to be that of diabase.

^jAlternate solution with bottom loading.

terrains range from 12 to 16 km (Table 1), only a slight increase from the results of *McGovern et al.* [2002].

2.4. Changes in Estimates of T_e and ρ_l

[8] To explain changes in the best fitting values for T_e and ρ_l , we note several effects of the gravity calculation correction applied here. First, compared with the results of *McGovern et al.* [2002], modeled admittances must be increased to match the observed admittances. In theory, such an increase may be accomplished by increasing either T_e or ρ_l . At short wavelengths, however, model admittance spectra for large T_e tend to converge, requiring that any increases in magnitude result from increased ρ_l . Thus, for features with high admittances such as the large volcanoes, ρ_l must be increased so that the corrected models fit the observed short-wavelength spectrum (e.g., Table 1). Second, since increasing ρ_l increases the admittance across the whole spectrum, T_e may need to be reduced by a corresponding amount to match the long-wavelength observations. Third, because of the wavelength dependence of the gravity reduction caused by the (previously omitted) upward continuation of the surface terms, the long-wavelength slopes of the revised admittance curves are lower than those in the original paper (Figure 1). Given that models with low T_e tend to have long-wavelength admittance curves with lower slopes than models with intermediate to high T_e (see Figure 1), the correction is likely to result in a lowering of elastic thickness estimates for certain regions. The interaction of these effects is seen most clearly at the large volcanoes. The first accounts for the increased densities found there, while the second and third account for the decreased T_e estimates (see Table 1). These effects were first seen in the results of *Belleguic et al.* [2004] for Olympus Mons.

3. Thermal History of Mars

[9] Although our new calculations allow a somewhat broader range of Martian thermal evolution models than reported by *McGovern et al.* [2002], the general finding of declining mantle heat flux with time still holds. Heat flux and thermal gradients for the Noachian and Noachian-Hesperian terrains (Figure 2) are very similar to our original results, as are those for Solis Planum and the Hesperian-Amazonian locations in Valles Marineris. These results are consistent with a rapid decline of mantle heat flux during the Noachian and a more modest subsequent decline, as deduced by *McGovern et al.* [2002].

[10] Whereas estimated heat fluxes and thermal gradients for the Amazonian volcanoes Olympus and Arsia Montes are similar to those previously calculated, those for Ascræus and Pavonis Montes are now seen to be unbounded above their lower limits. This finding is consistent with the inference of *Solomon and Head* [1990] that the thermal state of Mars in the Amazonian was characterized by large spatial variations. As noted above, however, the best fit elastic thickness values for Ascræus (32–46 km) and Pavonis Montes (12–78 km) are finite, unlike the $T_e = 0$ (Airy compensation) values that yield the best fits in the Noachian highlands. These best fit elastic thicknesses give bounds on heat flux and thermal gradient similar to those inferred in our previous paper (see the thickened lines in Figure 2). A thermal evolution in which the heat flux from

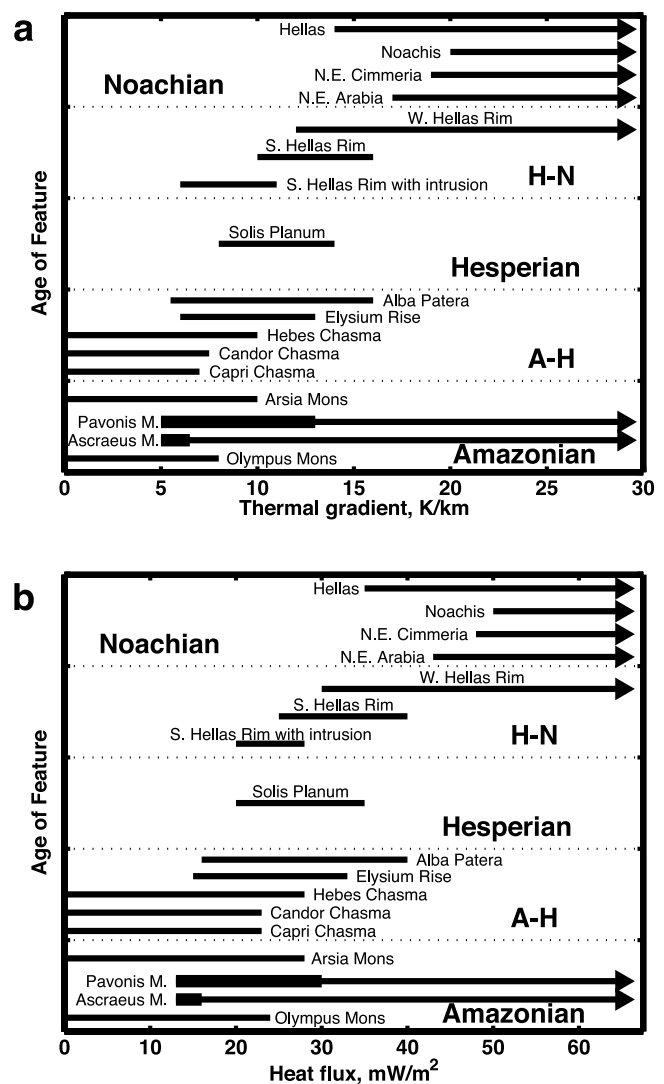


Figure 2. (a) Lithospheric thermal gradient dT/dz (in K/km) and (b) heat flux q (in mW/m^2) versus surface age for several regions on Mars. Three of the age subdivisions correspond to the Noachian, Hesperian, and Amazonian epochs (in order of decreasing age); the remaining two are used to identify features that exhibit surface unit ages spanning two epochs (see also Table 1). Within a given age subdivision, vertical positions give an approximate indication of the relative surface ages of features, although the development of a given pair of features may have overlapped in time. Arrows indicate that dT/dz or q have upper bounds that exceed the values shown in the figure. Thickened lines for Pavonis and Ascræus Montes indicate ranges in dT/dz and q for best fit models; for all other locations with arrows, the best fit values are unbounded. See color version of this figure in the HTML.

the Martian interior consistently declines with time [*Zuber et al.*, 2000; *McGovern et al.*, 2002; *McKenzie et al.*, 2002] thus remains the most likely scenario.

[11] **Acknowledgments.** We gratefully acknowledge V. Belleguic for pointing out the error in our original calculations and Associate Editor Francis Nimmo for constructive comments. This research was supported by

the National Aeronautics and Space Administration under grants NASW-4574 (to the Lunar and Planetary Institute, operated by the Universities Space Research Administration) and NAG 5-10165 (to the Carnegie Institution of Washington).

References

- Belleguic, V., M. Wieczorek, and P. Lognonné (2004), What can be learned about the Martian lithosphere from gravity and topography data?, *Lunar Planet. Sci.* [CD-ROM], XXXV, abstract 1741.
- Lemoine, F. G., D. E. Smith, D. D. Rowlands, M. T. Zuber, G. A. Neumann, D. S. Chinn, and D. E. Pavlis (2001), An improved solution of the gravity field of Mars (GMM-2B) from Mars Global Surveyor, *J. Geophys. Res.*, 106, 23,359–23,376.
- McGovern, P. J., S. C. Solomon, D. E. Smith, M. T. Zuber, M. Simons, M. A. Wieczorek, R. J. Phillips, G. A. Neumann, O. Aharonson, and J. W. Head (2002), Localized gravity/topography admittance and correlation spectra on Mars: Implications for regional and global evolution, *J. Geophys. Res.*, 107(E12), 5136, doi:10.1029/2002JE001854.
- McKenzie, D., D. N. Barnett, and D.-N. Yuan (2002), The relationship between Martian gravity and topography, *Earth Planet. Sci. Lett.*, 195, 1–16.
- McNutt, M. K. (1984), Lithospheric flexure and thermal anomalies, *J. Geophys. Res.*, 89, 11,180–11,194.
- Neumann, G. A., M. T. Zuber, M. A. Wieczorek, P. J. McGovern, F. G. Lemoine, and D. E. Smith (2004), The crustal structure of Mars from gravity and topography, *J. Geophys. Res.*, 109, doi:10.1029/2004JE002262, in press.
- Nimmo, F. (2002), Admittance estimates of mean crustal thickness and density at the Martian hemispheric dichotomy, *J. Geophys. Res.*, 107(E11), 5117, doi:10.1029/2000JE001488.
- Simons, M., S. C. Solomon, and B. H. Hager (1997), Localization of gravity and topography: Constraints on the tectonics and mantle dynamics of Venus, *Geophys. J. Int.*, 131, 24–44.
- Solomon, S. C., and J. W. Head (1990), Heterogeneities in the thickness of the elastic lithosphere of Mars: Constraints on heat flow and internal dynamics, *J. Geophys. Res.*, 95, 11,073–11,083.
- Thurber, C. H., and M. N. Toksöz (1978), Martian lithospheric thickness from elastic flexure theory, *Geophys. Res. Lett.*, 5, 977–980.
- Turcotte, D. L., R. J. Willemann, W. F. Haxby, and J. Norberry (1981), Role of membrane stresses in support of planetary topography, *J. Geophys. Res.*, 86, 3951–3959.
- Wieczorek, M. A., and R. J. Phillips (1998), Potential anomalies on a sphere: Applications to the thickness of the lunar crust, *J. Geophys. Res.*, 103, 1715–1724.
- Zuber, M. T., et al. (2000), Internal structure and early thermal evolution of Mars from Mars Global Surveyor topography and gravity, *Science*, 287, 1788–1793.